IEEE Access
Multidisciplinary ⋮ Rapid Review ⋮ Open Access Journal

Received 25 June 2023, accepted 11 July 2023, date of publication 17 July 2023, date of current version 24 July 2023.

Digital Object Identifier 10.1109/ACCESS.2023.3295896

RESEARCH ARTICLE

Fault Characteristic Analysis and a Novel Pilot Protection Scheme for Pole-to-Ground Fault in Flexible DC Distribution Network

HAO QI[1], WEI CHEN[1], (Member, IEEE), ZHENLAN DOU[2], (Member, IEEE), JIEXIANG HAN[1], PEI SUN[3], ZHE ZHANG[1], AND XIANGGEN YIN[1], (Senior Member, IEEE)

[1]School of Electrical and Electronic Engineering, Huazhong University of Science and Technology, Wuhan 430074, China
[2]State Grid Shanghai Municipal Electric Power Company, Shanghai 200023, China
[3]State Grid Shanghai Electric Power Research Institute, Shanghai 200437, China

Corresponding author: Wei Chen (weichen@hust.edu.cn)

This work was supported by the Science and Technology Project of State Grid Corporation of China under Grant 52094021N013.

ABSTRACT Due to the pseudo-bipolar structure of the flexible DC distribution network, the short-circuit current caused by a pole-to-ground fault is weak. The fault characteristics, particularly the steady-state fault characteristics, are not prominent. Therefore, pole-to-ground fault diagnosis and protection have become more challenging. This paper theoretically studies the short-circuit current characteristics of pole-to-ground fault in the flexible DC distribution network, derives the analytical expression of the short-circuit current, and analyzes the directional characteristics. Then, a novel pilot protection scheme based on fault direction comparison is proposed. This scheme compares the positive and negative half-wave integral values of the short-circuit current fault components to judge the fault direction. The fault directions on both sides of the feeder are obtained through the pilot protection channel, thereby distinguishing internal and external faults. The simulation results show that the proposed scheme can reliably identify the faulty feeder and has an excellent ability to perform with high transition resistance. Moreover, the scheme does not require sampling synchronization, which is easy to be applied in engineering.

INDEX TERMS Fault characteristics, fault direction judgment, flexible DC distribution network, pilot protection, pole-to-ground fault.

I. INTRODUCTION

Compared with the traditional AC distribution network, the flexible DC distribution network (FDCDN) has the advantages of large transmission capacity, low loss, and flexibility in operation and regulation [1], [2], [3], [4], [5]. It is incredibly convenient for flexible access to new energy power sources, energy storage equipment, and DC loads. Therefore, the FDCDN has become an important development direction for distribution network construction [6], [7]. In the actual operation of FDCDN, various faults may occur, mainly pole-to-pole (PTP) faults and pole-to-ground (PTG) faults, among which PTG faults are the most common [8]. Due to the pseudo-bipolar structure of the FDCDN, the neutral point of the converter is usually grounded through a large resistance. When a PTG fault occurs, the short-circuit current is mainly the capacitance current with small amplitude and complex characteristics, which brings severe challenges to fault diagnosis and protection. It has become a critical problem to be solved in the application of FDCDN engineering.

Various research has been carried out on PTG fault characteristic analysis and protection schemes. In studying PTG fault characteristics, [9] studies the voltage and current variation characteristics by simulation, but the theoretical analysis is insufficient. Zhao et al. [10] establishes a mathematical model of the grounding resistance circuit. However, this model ignores the influence of the distributed capacitance, so the transient fault characteristics are difficult to reflect. Dai et al. [11] analyzes the fault pole capacitance and grounding resistance circuits separately but ignores the

The associate editor coordinating the review of this manuscript and approving it for publication was Mauro Tucci.

non-fault pole capacitance discharge circuit. Li et al. [12] and Chen et al. [13] establish high-order mathematical models of the PTG fault. They also propose corresponding iterative solution methods that can accurately calculate the fault current in the time domain. However, the models are complex and cannot be solved analytically, so the short-circuit current's variation characteristics cannot be directly reflected.

Regarding PTG fault protection in FDCDN, Liu et al. [14] and Song et al. [15] propose using the change rate of fault current and bipolar voltage for faulty feeder identification. However, these methods rely on boundary elements at both ends of the feeder, which is challenging to be applied. Li et al. [16] uses the transient differential current to calculate the amount of transferred capacitance charges to locate the fault section. Bi et al. [17] proposes a PTG fault line identification method based on the short-time energy of the differential current. However, due to the high frequency of the fault current, these two methods have stringent requirements for sampling synchronization. They need dedicated optical fibers to form a communication link, which is costly and challenging to apply in FDCDN. Yang et al. [18] proposes a faulty feeder detection scheme based on the frequency domain characteristics of transient zero-mode current. However, the scheme puts high requirements on the sampling frequency. In addition, when a high-resistance ground fault occurs at the end of the feeder, the fault may be misjudged. He et al. [19] proposes a protection idea based on the initial polarity comparison of the current traveling waves. This scheme does not require strict sampling synchronization. However, due to the short effective time of the initial polarity, it puts high requirements on the immunity of the protection. In addition, the reference does not provide a specific protection criterion and implementation method, so its feasibility needs to be further verified. Sun et al. [20] proposes switching the grounding resistance to amplify the fault signature and thus reduce the difficulty of fault diagnosis. However, this method requires additional equipment at the grounding point, which increases the cost of construction, operation, and maintenance. Xu et al. [21] proposes injecting unique signals into the network by adjusting the MMC to facilitate fault location. However, this method is complicated to control and is only suitable for the radial network. It is challenging to apply in the double-terminal or multi-terminal network.

Given the above problems, this paper systematically studies the PTG fault current characteristics in the double-terminal FDCDN, considering the influence of grounding methods, distributed capacitance, and other factors. Then, this paper proposes a novel directional pilot protection scheme based on comparing the integral values of the short-circuit current fault components to solve problems such as stringent sampling synchronization, high sampling frequency, and insufficient applicability in multi-terminal DC distribution networks. Finally, a simulation model is built in PSCAD to verify the correctness of the analysis method and the performance of the directional pilot protection scheme.

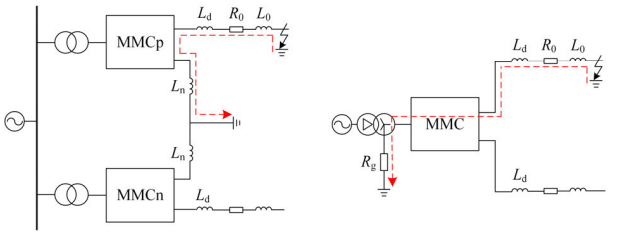

(a)Flexible DC transmission network (true-bipolar structure)

(b)Flexible DC distribution network (pseudo-bipolar structure)

FIGURE 1. Schematic diagram of PTG fault in flexible DC network.

II. PTG FAULT CHARACTERISTIC ANALYSIS IN FDCDN

A. FDCDN STRUCTURE

The flexible DC transmission network generally adopts the true-bipolar structure, as shown in Fig. 1(a). When a PTG fault occurs, the ground return can help form the current circuit. The large amplitude of the fault current is conducive to fault detection. In contrast, the FDCDN generally adopts the pseudo-bipolar structure, as shown in Fig. 1(b). The neutral point of the converter is grounded through a large resistance (2∼3 kΩ) to limit the grounding current (within 10 A), and the safety of personnel and equipment near the fault point can be ensured [20]. The short-circuit current is mainly capacitive, making fault detection difficult.

In the FDCDN, the PTG fault characteristics are related to many factors, such as grid topology, converter structure, grounding method, and grounding element parameters. The double-terminal network can better meet the requirements of economy and power supply reliability. It is easy and flexible to operate and control and has been widely used in engineering [6]. Therefore, this paper carries out the study in the context of the double-terminal DC distribution network shown in Fig. 2. In the figure, the modular multilevel converter (MMC) realizes conversion between AC and DC. The MMC adopts a mixed structure of full-bridge and half-bridge submodules to achieve fault ride-through operation. At the outlet of the MMC, the current-limiting reactor L_d is installed to limit the short-circuit current of the PTP fault. B1∼B4 are DC buses, and L1∼L3 are feeders. i_{01p}, i_{01n}, i_{02p}, and i_{02n} are the positive and negative measuring currents of MMC1 and MMC2, respectively. i_{kjp} and i_{kjn} ($k, j = 1, 2, 3, 4$) are the feeder's positive and negative measuring currents between bus Bk and Bj. It should be noted that the relay protection requirements define the positive direction of the measuring current from the bus to the line.

The DC distribution network generally adopts the pseudo-bipolar structure. When the secondary winding of the converter adopts star wiring form, its neutral point is grounded through a large resistance, as shown in Fig. 1(b). If the secondary side of the converter is a delta winding, the neutral point can be constructed by a star-shaped reactance and grounded through large resistance. When a PTG fault occurs, the two grounding methods may lead to similar fault

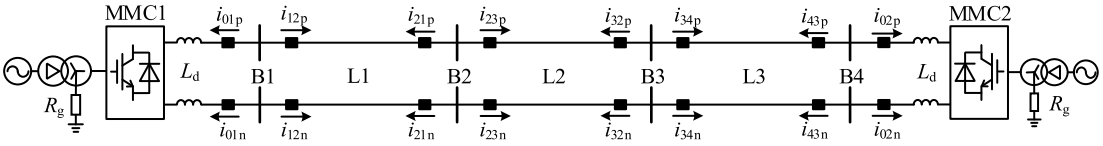

FIGURE 2. Structure of the double-terminal FDCDN.

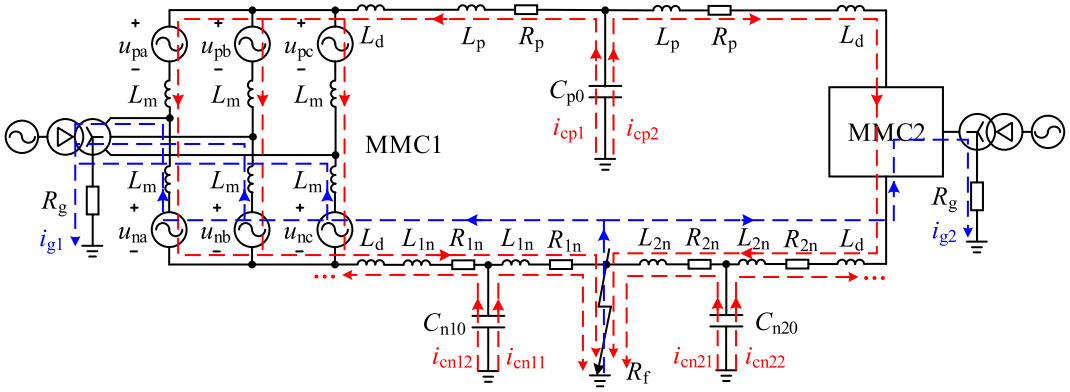

FIGURE 3. Equivalent model of negative PTG fault.

characteristics. In this paper, the neutral point is grounded through large resistance as an example to study the PTG fault characteristics.

B. EQUIVALENT MODEL OF PTG FAULT

In the PTG fault characteristic analysis, this paper takes the negative PTG fault on the feeder L2 as an example (as shown in Fig. 2). The equivalent model is shown in Fig. 3. The T-type equivalent circuit is used for DC feeders. For the positive line, C_{p0} is the total equivalent capacitance; L_p and R_p are the equivalent inductance and resistance, respectively. L_d is the current-limiting inductance. For the negative line, the feeders between the fault point and the two MMCs are equivalent to two T-type circuits. C_{n10} and C_{n20} are the equivalent capacitances of the feeders on both sides of the fault point; L_{1n}, R_{1n}, L_{2n}, and R_{2n} are the equivalent inductances and resistances, respectively. R_g is the grounding resistance of the neutral point; L_m is the bridge arm inductance of MMC1. $u_{p\varphi}$ and $u_{n\varphi}$ (φ = a, b, c) are the output voltages of the upper and lower bridge arms of MMC1, respectively.

As shown in Fig. 3, when a negative PTG fault occurs in the network, the distributed capacitance of the non-fault pole (positive pole) and the fault pole (negative pole) will discharge to the fault point. i_{cp1} and i_{cp2} are the positive capacitance currents, and i_{cn11}, i_{cn12}, i_{cn21}, and i_{cn22} are the negative capacitance currents. The fault point will also form a fault circuit with the convertor through the grounding resistance, thus forming a steady-state short-circuit current as i_{g1} and i_{g2}. Since the neutral grounding resistance is generally 2∼3 kΩ, the current of this circuit, that is, the steady-state short-circuit current, is only 3∼5 A. Therefore, its influence can be ignored.

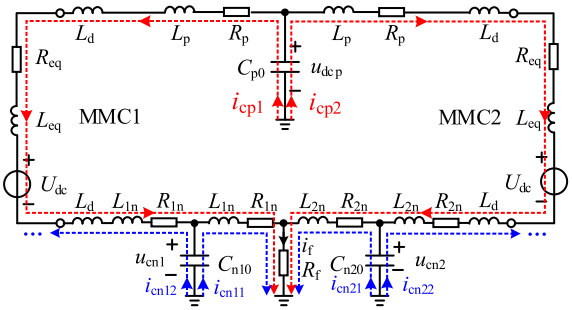

FIGURE 4. Equivalent circuit of negative PTG fault.

C. ANALYTICAL ANALYSIS OF PTG FAULT CHARACTERISTICS

In the case of neglecting the steady-state short-circuit current, Fig. 4 shows the equivalent circuit of the model in Fig. 3. The fault characteristics are mainly influenced by the distributed capacitance discharge circuit. In Fig. 4, R_{eq} and L_{eq} are MMC's equivalent resistance and inductance, respectively. A PTG fault will not affect the operation of MMC so that the MMCs can be replaced by the voltage source U_{dc}. The meanings of other parameters are the same as those in Fig. 3.

As shown in Fig. 4, the circuit parameters on both sides of the negative equivalent capacitance are significantly different. Due to the effect of L_d, when the capacitance discharges through the positive line (as i_{cn12} and i_{cn22}), the inductance of the discharge circuit is relatively large. Furthermore, the discharge current of C_{n10} (i_{cn12}) and C_{n20} (i_{cn22}) weaken each other in the positive line. Therefore, the negative (fault pole) capacitance mainly discharges to the fault point. So the current flowing through the protection on both sides of the negative line is mainly the positive (non-fault pole)

capacitance current. To reduce the network order and simplify the analysis process, we ignore the influence of the fault pole capacitance in the fault current solution. Fig. 5(a) shows the discharge circuit of the non-fault pole (positive pole) capacitance. $L_{\Sigma p1}$, $R_{\Sigma p1}$, $L_{\Sigma p2}$, and $R_{\Sigma p2}$ are the total inductance and resistance of the two discharge circuits, which can be calculated from Fig. 4. Fig. 5(b) shows the discharge circuit of the fault pole (negative pole) capacitance.

For the discharge current of the non-fault pole (positive pole) distributed capacitance, the simplified discharge circuit is a third-order network whose network equation is:

$$\begin{cases} C_{p0}\dfrac{du_{dcp}}{dt} = -i_{cp1} - i_{cp2} \\ L_{\Sigma p1}\dfrac{di_{cp1}}{dt} + R_{\Sigma p1}i_{cp1} + U_{dc} = L_{\Sigma p2}\dfrac{di_{cp2}}{dt} + R_{\Sigma p2}i_{cp2} + U_{dc} \\ L_{\Sigma p1}\dfrac{di_{cp1}}{dt} + R_{\Sigma p1}i_{cp1} + U_{dc} = u_{dcp} - \left(i_{cp1} + i_{cp2}\right)R_f \end{cases} \tag{1}$$

Before the fault occurs, the initial value of the discharge current is zero. The Laplace transform of (1) can be obtained as:

$$\begin{bmatrix} 1 & 1 & sC_{p0} \\ sL_{\Sigma p1} + R_{\Sigma p1} & -\left(sL_{\Sigma p2} + R_{\Sigma p2}\right) & 0 \\ sL_{\Sigma p1} + R_{\Sigma p1} + R_f & R_f & -1 \end{bmatrix} \begin{bmatrix} I_{cp1}(s) \\ I_{cp2}(s) \\ U_{dcp}(s) \end{bmatrix} = \begin{bmatrix} C_{p0}U_{dc}/2 \\ 0 \\ -U_{dc}/s \end{bmatrix} \tag{2}$$

Solving (2), we can obtain the complex frequency domain expression of the current as:

$$\begin{bmatrix} I_{cp1}(s) \\ I_{cp2}(s) \end{bmatrix} = \frac{1}{G(s)} \begin{bmatrix} -C_{p0}U_{dc}\left(sL_{\Sigma p2} + R_{\Sigma p2}\right)/2 \\ -C_{p0}U_{dc}\left(sL_{\Sigma p1} + R_{\Sigma p1}\right)/2 \end{bmatrix} \tag{3}$$

In the formula, $G(s)$ is expressed as:

$$\begin{cases} G(s) = As^3 + Bs^2 + Cs + D \\ A = L_{\Sigma p1}L_{\Sigma p2}C_{p0} \\ B = \left[\left(L_{\Sigma p1} + L_{\Sigma p2}\right)R_f + R_{\Sigma p1}L_{\Sigma p2} + R_{\Sigma p2}L_{\Sigma p1}\right]C_{p0} \\ C = L_{\Sigma p1} + L_{\Sigma p2} + C_{p0}\left(R_{\Sigma p1}R_f + R_{\Sigma p2}R_f + R_{\Sigma p1}R_{\Sigma p2}\right) \\ D = R_{\Sigma p1} + R_{\Sigma p2} \end{cases} \tag{4}$$

The circuit resistances $R_{\Sigma p1}$ and $R_{\Sigma p2}$ comprise the feeder resistance and the switching element on-resistance. The feeder resistance is much smaller than the feeder inductance. Therefore, the effect of the feeder resistance can be ignored, and $G(s)$ can be simplified as:

$$G(s) = L_{\Sigma p1}L_{\Sigma p2}C_{p0}s^3 + \left(L_{\Sigma p1} + L_{\Sigma p2}\right)R_fC_{p0}s^2 + \left(L_{\Sigma p1} + L_{\Sigma p2}\right)s \tag{5}$$

Let $L_{\Sigma eq} = L_{\Sigma p1}L_{\Sigma p2}/(L_{\Sigma p1} + L_{\Sigma p2})$. Substituting (5) into (3), we can obtain the complex frequency domain expression

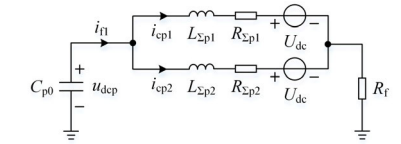

(a) Discharge circuit of the non-fault pole capacitance

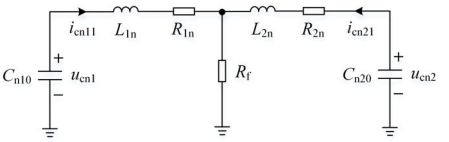

(b) Discharge circuit of the fault pole capacitance

FIGURE 5. Simplified discharge circuit of distributed capacitance.

of the fault current as:

$$\begin{bmatrix} I_{cp1}(s) \\ I_{cp2}(s) \end{bmatrix} = \frac{1}{L_{\Sigma eq}C_{p0}s^2 + R_fC_{p0}s + 1} \begin{bmatrix} \frac{-L_{\Sigma p2}C_{p0}U_{dc}}{2(L_{\Sigma p1}+L_{\Sigma p2})} \\ \frac{-L_{\Sigma p1}C_{p0}U_{dc}}{2(L_{\Sigma p1}+L_{\Sigma p2})} \end{bmatrix} \tag{6}$$

Doing the inverse Laplace transform on (6), we can obtain the discharge current of the positive pole as:

$$\begin{aligned} i_{cp1} &= \frac{L_{\Sigma p1}}{L_{\Sigma p2}}i_{cp2} \\ &= \begin{cases} \dfrac{-L_{\Sigma p2}C_{p0}U_{dc}\omega_0^2}{2\omega_{p1}\left(L_{\Sigma p1} + L_{\Sigma p2}\right)}e^{-\alpha_p t}\sin\left(\omega_{p1}t\right), \\ \qquad R_f < 2\sqrt{L_{\Sigma eq}/C_{p0}} \\ \dfrac{-L_{\Sigma p2}C_{p0}U_{dc}\omega_0^2}{2\left(L_{\Sigma p1} + L_{\Sigma p2}\right)}te^{-\alpha_p t},\ R_f = 2\sqrt{L_{\Sigma eq}/C_{p0}} \\ \dfrac{-L_{\Sigma p2}C_{p0}U_{dc}\omega_0^2}{2\omega_{p2}\left(L_{\Sigma p1} + L_{\Sigma p2}\right)}e^{-\alpha_p t}\sinh\left(\omega_{p2}t\right), \\ \qquad R_f > 2\sqrt{L_{\Sigma eq}/C_{p0}} \end{cases} \end{aligned} \tag{7}$$

Among the formula: $\alpha_p = R_f/(2L_{\Sigma eq})$, $\omega_{p1} = (\omega_0^2 - \alpha_p^2)^{1/2}$, $\omega_{p2} = (\alpha_p^2 - \omega_0^2)^{1/2}$, $\omega_0 = (L_{\Sigma eq}C_{p0})^{-1/2}$.

From (7), with different transition resistance, the discharge current can be divided into underdamped, overdamped, and critically damped. In the underdamped state, the current is a decaying sine wave with a negative initial half-wave, so the area of the negative half-wave must be larger than the area of the positive half-wave. In the critically damped and overdamped states, the current is constantly negative. The schematic waveform diagram is shown in Fig. 6(a).

For the current characteristics of the fault-pole (negative pole) distributed capacitance, from Fig. 5(b), we can see that the circuit inductance is just the feeder inductance. It is much smaller than the series inductance in Fig. 5(a). Moreover, the discharge frequency of the RLC equivalent circuit mainly depends on the formula $1/\sqrt{LC}$. Therefore, the fault-pole capacitance current has a high oscillation frequency and is challenging to use. In the protection design, the influence

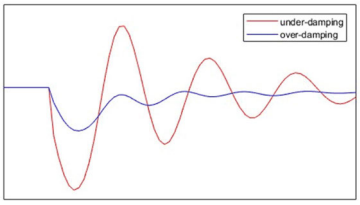

(a) Schematic waveform diagram of the negative PTG fault current

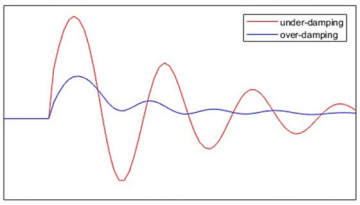

(b) Schematic waveform diagram of the positive PTG fault current

FIGURE 6. Schematic waveform diagram of the non-fault pole discharge current with different transition resistance.

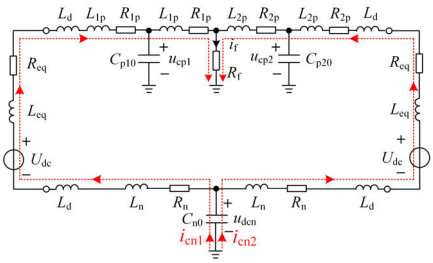

(a) Equivalent circuit

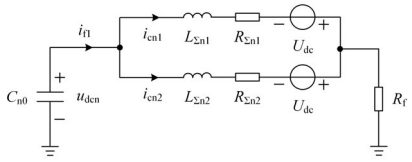

(b) Simplified discharge circuit of non-fault pole distributed capacitance

FIGURE 7. Equivalent circuit of positive PTG fault.

of the fault pole capacitance current can be eliminated by filtering to facilitate the engineering application.

Similarly, when a positive PTG fault occurs, the discharge circuit of the non-fault pole (negative pole) capacitance is shown in Fig. 7. The difference between Fig. 5(a) and Fig. 7(b) is only the sign of U_{dc}. Therefore, the characteristics of the negative capacitance current are opposite to the above-mentioned situation. When the current is underdamped, it is a decaying sine wave with a positive initial half-wave, so the area of the positive half-wave must be larger than the area of the negative half-wave. In the critically damped and over-damped states, the current is always positive. The schematic waveform diagram is shown in Fig. 6(b). Therefore, the non-fault pole capacitance current has explicit directional characteristics.

In summary, when a PTG fault occurs in FDCDN, the steady-state information of the fault current is insufficient. The amplitude of the current is small. Therefore, only the transient capacitance current can be used for fault detection. Furthermore, the non-fault pole capacitance current has a low frequency and a relatively long duration, which can be mainly used for fault protection. The analysis above shows that the difference between the positive and negative half-wave amplitudes is evident when a forward or reverse fault occurs. We can use these characteristics to judge the fault direction and then construct the directional pilot protection scheme to identify the faulty feeder reliably.

III. DIRECTIONAL PILOT PROTECTION SCHEME BASED ON THE DOUBLE INTEGRATION OF CURRENT FAULT COMPONENTS

The directional pilot protection comprises the fault starting element, the fault pole selection element, and the fault direction judgment element.

A. FAULT STARTING ELEMENT CRITERION

After the PTG fault occurs, the voltage traveling wave propagates from the fault point to both sides of the line, causing the positive and negative voltages to increase or decrease rapidly. Therefore, the protection can be activated by using the rapid change of the voltages. The specific method is to calculate the variation of the positive and negative voltages. When one exceeds the set threshold for three consecutive points, the protection will be activated immediately, and the fault time will be determined accordingly. The voltage variation starting criterion is:

$$\begin{cases} \max\left\{\Delta u_{dcp}, \Delta u_{dcn}\right\} \geq \Delta U_{set} \\ \Delta u_{dcp}(k) = \left| \begin{array}{l} \left|u_{dcp}(k) - u_{dcp}(k-M)\right| \\ -\left|u_{dcp}(k-M) - u_{dcp}(k-2M)\right| \end{array} \right| \\ \Delta u_{dcn}(k) = \left| \begin{array}{l} \left|u_{dcn}(k) - u_{dcn}(k-M)\right| \\ -\left|u_{dcn}(k-M) - u_{dcn}(k-2M)\right| \end{array} \right| \end{cases} \tag{8}$$

In the formula, Δu_{dcp} is the positive voltage variation. Δu_{dcn} is the negative voltage variation. u_{dcp} is the positive voltage sampling value. u_{dcn} is the negative voltage sampling value. k is the number of sampling points. M is the number of samples in the mutation calculation data window, whose typical value can be 10ms. ΔU_{set} is the set threshold of the voltage variation, which can be taken as $\Delta U_{set} = 0.1 U_{dcN}$, and U_{dcN} is the rated voltage between poles.

B. FAULT POLE SELECTION ELEMENT CRITERION

DC distribution network faults mainly include PTP and PTG faults, where the PTG faults can be further divided into positive and negative PTG faults. After the protection is activated, different protection criteria shall be adopted according to different short-circuit forms.

When the DC distribution network operates normally, the voltage between poles is U_{dcN}. The positive PTG voltage is $U_{dcN}/2$, and the negative PTG voltage is $-U_{dcN}/2$. When a

PTG fault occurs, the fault pole is clamped to zero potential, and the voltage of the non-fault pole rises to twice its original value. The voltage between poles remains unchanged. When a PTP fault occurs, the voltage of the two poles drops together. These features can be used to distinguish between PTP faults and PTG faults. The criterion for PTP fault is:

$$\left|u_{\mathrm{dcp}}\right| < K_{rel-1} \times \frac{U_{\mathrm{dcN}}}{2} \cap \left|u_{\mathrm{dcn}}\right| < K_{rel-1} \times \frac{U_{\mathrm{dcN}}}{2} \quad (9)$$

The short-circuit current of PTP fault is relatively large, and various protection schemes have been proposed [22], [23], [24]. Once a PTP fault is judged to have occurred, the relevant PTP fault protection scheme can be used for fault location, and the tripping operation will remove the fault. The details are omitted in this paper.

If the criterion for PTP fault (formula (9)) is not satisfied, the pole selection for PTG faults will be performed. It is not difficult to prove that when the positive pole is shorted to ground, the positive PTG voltage drops from $U_{\mathrm{dcN}}/2$ to zero, and the negative PTG voltage drops from $-U_{\mathrm{dcN}}/2$ to $-U_{\mathrm{dcN}}$. When the negative pole is shorted to the ground, the negative PTG voltage rises from $-U_{\mathrm{dcN}}/2$ to zero, and the positive PTG voltage rises from $U_{\mathrm{dcN}}/2$ to U_{dcN}. These voltage variation characteristics can be used for the pole selection criterion.

The positive pole selection criterion is:

$$\left|u_{\mathrm{dcp}}\right| < K_{rel-1} \times \frac{U_{\mathrm{dcN}}}{2} \cap \left|u_{\mathrm{dcn}}\right| > K_{rel-2} \times \frac{U_{\mathrm{dcN}}}{2} \quad (10)$$

The negative pole selection criterion is:

$$\left|u_{\mathrm{dcn}}\right| < K_{rel-1} \times \frac{U_{\mathrm{dcN}}}{2} \cap \left|u_{\mathrm{dcp}}\right| > K_{rel-2} \times \frac{U_{\mathrm{dcN}}}{2} \quad (11)$$

Among the formula, K_{rel-1} and K_{rel-2} are reliability coefficients. Taking the 20% reliability threshold, we can take the typical values as $K_{rel-1} = 0.8$ and $K_{rel-2} = 1.2$.

Once the fault pole is determined, the measuring current of the fault pole can be used to identify the fault direction.

C. FAULT DIRECTION JUDGMENT METHOD BASED ON THE DOUBLE INTEGRATION OF CURRENT FAULT COMPONENTS

The fault analysis in this paper shows that when a PTG fault occurs, the non-fault pole capacitance current (that is, short-circuit current fault component) has clear directional characteristics. The fault direction can be identified according to the difference in the amplitude of the positive and negative half-waves. Therefore, this paper proposes to compare the positive and negative half-wave integral values to judge the fault direction. This method could determine the fault direction based on only the local current information and has no special requirements for sampling synchronization on both sides of the feeder. It is easy to apply in engineering.

In order to avoid the influence of the fault-pole capacitance current, it is necessary to perform low-pass filtering on the measuring current. The frequency of the fault pole capacitance current is much higher than that of the non-fault pole capacitance current, and only the latter is needed for protection. In the design of the low-pass filter, we can set the cut-off frequency higher than the frequency of the non-fault pole capacitance current to reduce the loss of information.

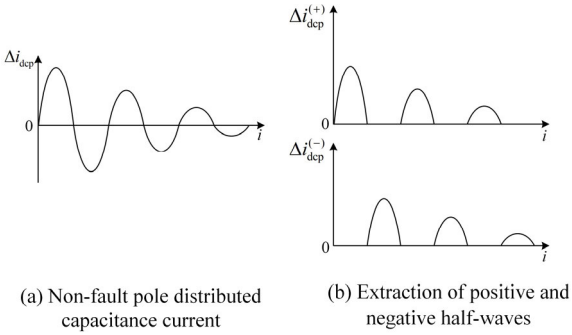

(a) Non-fault pole distributed capacitance current

(b) Extraction of positive and negative half-waves

FIGURE 8. Schematic diagram of positive and negative half-wave extraction with a positive PTG fault.

The fault direction judgment method is as follows:

(1) Extraction of fault components: When the fault occurs, we first subtract the pre-fault current from the measuring current to obtain the current fault component. Taking the positive current as an example, the calculation method of the fault component is:

$$\begin{cases} \Delta i_{\mathrm{dcp}}(i) = i_{\mathrm{dcp}}(i) - I_{0\mathrm{p}} \\ I_{0\mathrm{p}} = \dfrac{1}{N}\displaystyle\sum_{k=0}^{N} i_{\mathrm{dcp}(0)}(k) \end{cases} \quad (12)$$

Among the formula, $i_{\mathrm{dcp}}(i)$ is the positive current sampling value. $\Delta i_{\mathrm{dcp}}(i)$ is the calculated positive current fault component. $I_{0\mathrm{p}}$ is the positive load current before the fault, calculated by the mean value of $i_{\mathrm{dcp}(0)}(k)$, the sampling value of the pre-fault current. N is the number of sampling points in the mean calculation data window, and this paper takes it as 5.

(2) Calculation of positive and negative half-wave sampling values: In the under-damped case, the short-circuit current provided by the non-fault pole capacitance is an attenuated sine wave, as shown in Fig. 8(a). For the positive measuring current, the calculation methods of the positive and negative half-wave sampling values are as follows:

$$\begin{cases} \Delta i_{\mathrm{dcp}}^{(+)}(i) = (\Delta i_{\mathrm{dcp}}(i) + \left|\Delta i_{\mathrm{dcp}}(i)\right|)/2 \\ \Delta i_{\mathrm{dcp}}^{(-)}(i) = (\left|\Delta i_{\mathrm{dcp}}(i) - \left|\Delta i_{\mathrm{dcp}}(i)\right|\right|)/2 \end{cases} \quad (13)$$

Among the formula, $\Delta i_{\mathrm{dcp}}^{(+)}(i)$ is the positive half-wave sampling value of the current fault component. $\Delta i_{\mathrm{dcp}}^{(-)}(i)$ is the absolute value of the negative half-wave sampling value. The calculation result of (13) is shown in Fig. 8(b).

The positive and negative half-wave extraction methods for the negative short-circuit current fault component are analogous, that is:

$$\begin{cases} \Delta i_{\mathrm{dcn}}^{(+)}(i) = (\Delta i_{\mathrm{dcn}}(i) + |\Delta i_{\mathrm{dcn}}(i)|)/2 \\ \Delta i_{\mathrm{dcn}}^{(-)}(i) = (|\Delta i_{\mathrm{dcn}}(i) - |\Delta i_{\mathrm{dcn}}(i)||)/2 \end{cases} \quad (14)$$

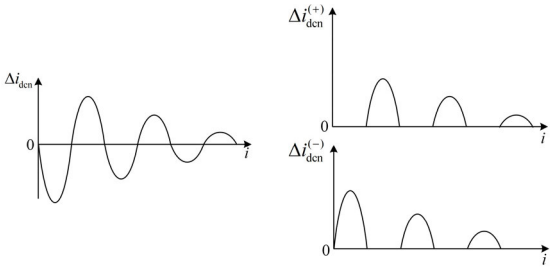

(a) Non-fault pole distributed capacitance current

(b) Extraction of positive and negative half-waves

FIGURE 9. Schematic diagram of positive and negative half-wave extraction with a negative PTG fault.

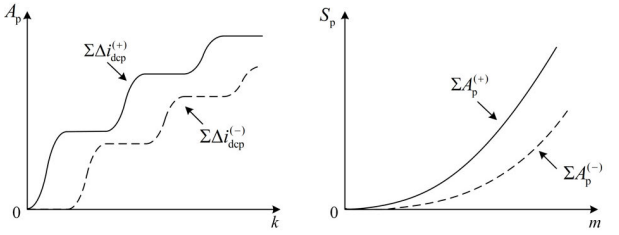

(a) Schematic diagram of primary integral values

(b) Schematic diagram of double integral values

FIGURE 10. Schematic diagram of the fault direction criterion.

Among the formula, $\Delta i_{dcn}(i)$ is the calculated negative current fault component. $\Delta i_{dcn}^{(+)}(i)$ is the positive half-wave sampling value of the current fault component. $\Delta i_{dcn}^{(-)}(i)$ is the absolute value of the negative half-wave sampling value. The schematic diagram is shown in Fig. 9.

(3) The fault direction criterion based on comparing positive and negative half-wave integral values: The positive and negative half-waves of the measuring currents need to be integrated to obtain the graph area formed by each waveform and the horizontal axis. The time interval is normalized to facilitate the comparison of integration results, so the summation operation is done directly on the sampling values. Taking the positive short-circuit current as an example, the integral calculation is as follows:

$$\begin{cases} A_{pk}^{(+)} = \sum_{i=1}^{k} \Delta i_{dcp}^{(+)}(i) \\ A_{pk}^{(-)} = \sum_{i=1}^{k} \Delta i_{dcp}^{(-)}(i) \end{cases} \tag{15}$$

Among the formula, $A_{pk}^{(+)}$ and $A_{pk}^{(-)}$ are the cumulative summation of $\Delta i_{dcn}^{(+)}(i)$ and $\Delta i_{dcn}^{(-)}(i)$. They can be called 'primary integral values.' The subscripts i and k represent the sampling value serial number and the integral data window length, respectively.

From Fig. 10(a), the primary integral values of positive and negative half-wave rise with time alternately, and the two values are relatively close at some moments. Therefore, to improve the reliability of fault direction judgment, the integral values are integrated again as:

$$\begin{cases} S_{pm}^{(+)} = \sum_{k=1}^{m} A_{pk}^{(+)} \\ S_{pm}^{(-)} = \sum_{k=1}^{m} A_{pk}^{(-)} \end{cases} \tag{16}$$

Among the formula, $S_{pm}^{(+)}$ and $S_{pm}^{(-)}$ are the cumulative summation of the primary integral values. They can be called 'double integral values.' The subscript m represents the integral data window length of the double integration. Compared with the primary integral values, the double integral values shown in Fig. 10(b) increase the difference between the positive and negative half-waves, which helps to improve the performance of the direction judgment elements.

According to the fault characteristic analysis mentioned above, when a positive fault occurs, the positive measuring current has a positive initial half-wave (under-damping) or is constantly positive (critical damping and over-damping). So when a forward fault occurs, the positive half-wave integral value of the short-circuit current is larger than the negative half-wave integral value. Therefore, the positive direction criterion for positive PTG fault is:

$$S_p^{(+)} \geq K_{rel-s} S_p^{(-)} \Rightarrow \text{a forward fault} \tag{17}$$

In the formula, K_{rel-s} is the reliability coefficient. Taking the 25% reliability threshold, we can take the typical value as 1.25.

If the result of pole selection shows that a PTG fault occurs in the negative pole, the fault direction can be judged by the measuring current of the negative pole. The positive direction criterion is:

$$S_n^{(-)} \geq K_{rel-s} S_n^{(+)} \Rightarrow \text{a forward fault} \tag{18}$$

D. THE DIRECTIONAL PILOT PROTECTION SCHEME

The directional pilot protection can be constructed according to the fault direction judgment results. If the directional elements on both sides of the feeder judge that a fault occurs in the positive direction, the feeder is faulty. If one side judges the fault is in the positive direction and the other judges the fault is in the reverse direction, the feeder is not faulty. For MMC lead wires, internal and external faults can be distinguished based on the fault pole selection result and the judgment result of the lead wire directional element. There is no need to obtain the information from other elements. Fig. 11 shows the specific implementation flow chart. Once the protection is activated, the fault pole selection element has to determine whether it is a PTP or PTG fault. The current characteristics of PTP and PTG faults are so different that we have to use different protection schemes to protect the network well. Suppose a positive or negative PTG fault is judged to have occurred:

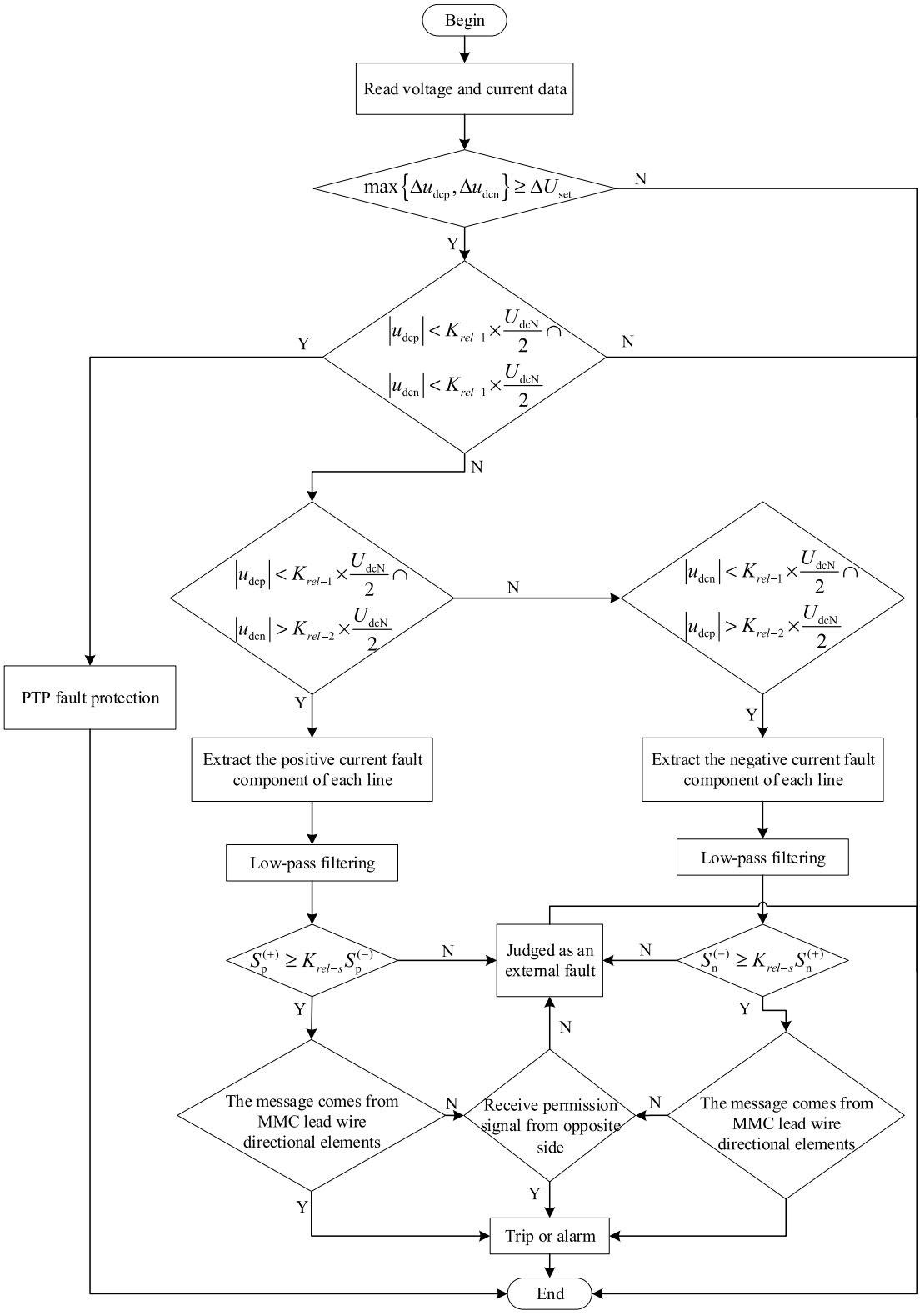

FIGURE 11. Flow chart of the protection scheme.

(1) The fault component of the fault-pole measuring current has to be extracted.

(2) A low-pass filtering method has to be used to eliminate the influence of the fault pole capacitance current.

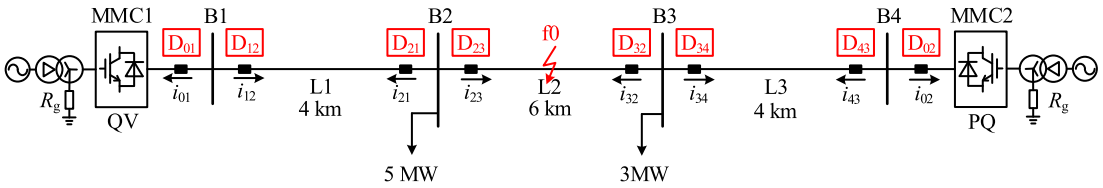

FIGURE 12. Structure of the simulation system.

TABLE 1. Key parameters of the simulation system.

Parameter (Unit)	Value	Parameter (Unit)	Value	Parameter (Unit)	Value
Transformer capacity (MVA)	20	Primary voltage (kV)	110	Secondary voltage (kV)	10.5
Transformer leakage reactance (pu)	0.1	Grounding resistance (kΩ)	2	Current-limiting inductance (mH)	5
MMC capacity (MVA)	20	Number of half-bridge submodules	5	Number of full-bridge submodules	5
Sub-module capacitance (mF)	8	Bridge arm inductance (mH)	8	Bridge arm resistance (Ω)	0.1
C_0 of feeder (μF/km)	0.15	L_0 of feeder (mH/km)	0.25	R_0 of feeder (Ω/km)	0.02
Lenth of L1 (km)	4	Lenth of L2 (km)	6	Lenth of L3 (km)	4

(3) We can use the double integral values to judge the fault direction, select the faulty line according to the protection action logic shown in Fig. 11, and issue a trip or alarm signal as needed.

According to the proposed protection scheme, the action time of the protection mainly depends on the length of the double integration data window. We could set the integration data window length to 3 ms considering a certain reliability margin. Therefore, the shortest action time of the protection is 3 ms.

When the main protection or the circuit breaker fails to operate, the fault cannot be removed reliably. In addition to the proposed directional pilot protection, it is also necessary to configure the corresponding backup protection. Due to the small PTG fault current, the overcurrent protection principle is hard to be used for backup protection. We can use the fault direction judgment method proposed in this paper and a time delay to form the backup protection. When the fault occurs, and the directional element judges it as a forward fault, the main protection must operate immediately. If the fault pole voltage has not returned to normal and the fault has not been removed after the set time delay, the backup protection will operate to remove the fault. The set value of the time delay can adopt the coordination method of the traditional overcurrent protection. That is, the protections in the same direction coordinate in a step-by-step manner to ensure the selectivity of the protection.

IV. SIMULATION

A. SIMULATION OF PTG FAULT CHARACTERISTICS

The double-terminal DC distribution network simulation model shown in Fig. 12 is built in PSCAD/EMTDC to verify the theoretical analysis conclusions of the PTG fault current. The critical parameters of the simulation system are given in Table 1. The parameters of the MMC and the converters on both sides of the system are the same. MMC1 uses constant DC voltage control, and MMC2 uses constant power control with an active command of 12 MW in the simulation system. Bus B2 is connected to a 5 MW load, and Bus B3 is connected to a 3 MW load. D_{0n} ($n = 1, 2$) is the MMC outgoing directional element, and D_{ij} ($i, j = 1, 2,3,4$) is the directional element on both sides of the feeder connecting bus Bi to Bj.

A metallic ground fault f0 is set at the midpoint of the positive line of L2, and Fig. 13 shows the simulation waveforms and theoretical calculation results of the currents. Fig. 13 (a)∼(c) correspond to the fault currents on both sides of L1∼L3, respectively. The fault simulation waveforms agree with the theoretical calculation results, proving the correctness of the analytical analysis.

As Fig. 13(a), for the protection of L1 close to MMC1, the fault f0 is a forward fault. The measuring current (i_{12p}) is a decaying sine wave, and the initial half wave is positive, consistent with the theoretical analysis. For the protection close to the fault point, fault f0 is a reverse fault. The measuring current (i_{21p}) contains the discharge current of the negative distributed capacitance and the high-frequency positive capacitance current of feeder L1. Once the fault current is filtered, the measuring current will be mainly the capacitance current provided by the negative pole (non-fault pole), which is still an attenuated sine wave with a negative initial half-wave. The result is also the same as the theoretical analysis.

As seen in Fig. 13(b) and 13(c), for feeder L2 with internal faults, the measuring currents on both sides are attenuated sine waves, and the initial half-wave is positive

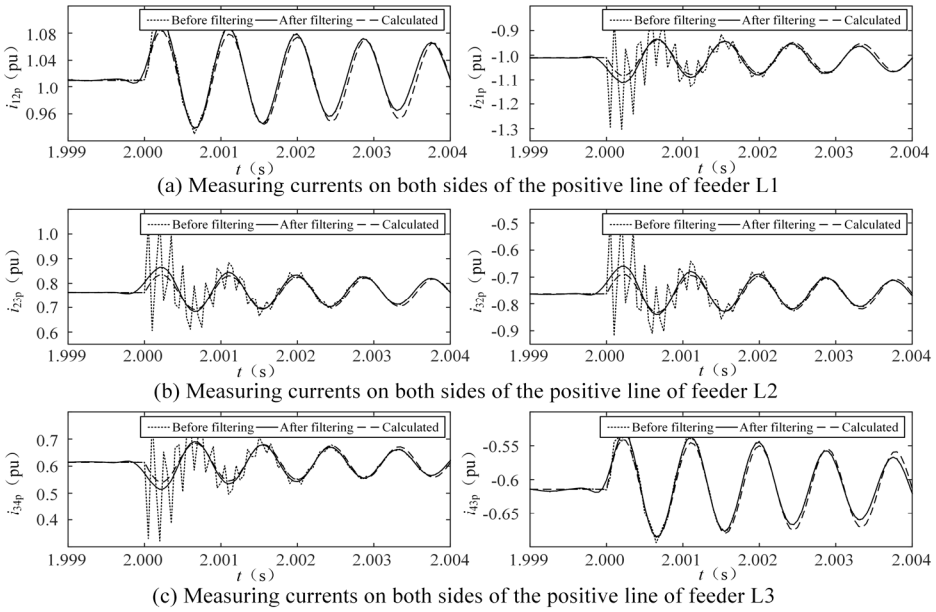

FIGURE 13. Simulation waveforms and calculation results of positive metallic ground fault.

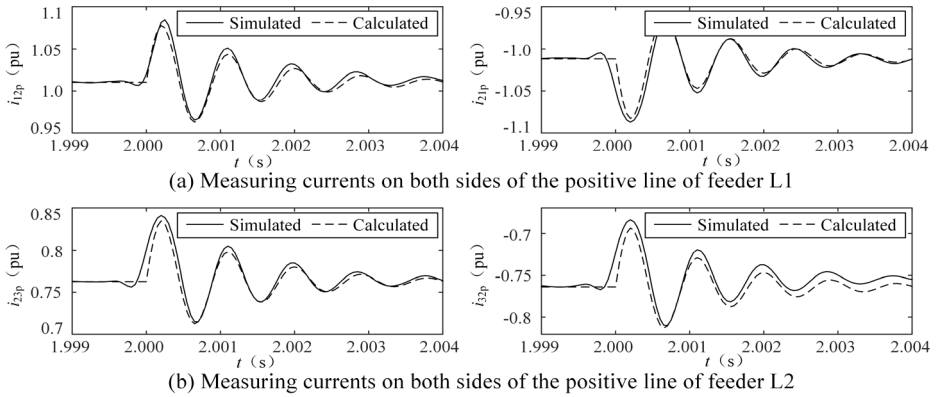

FIGURE 14. Simulation waveforms and calculation results of the positive pole-to-ground fault with 10-ohm transition resistance.

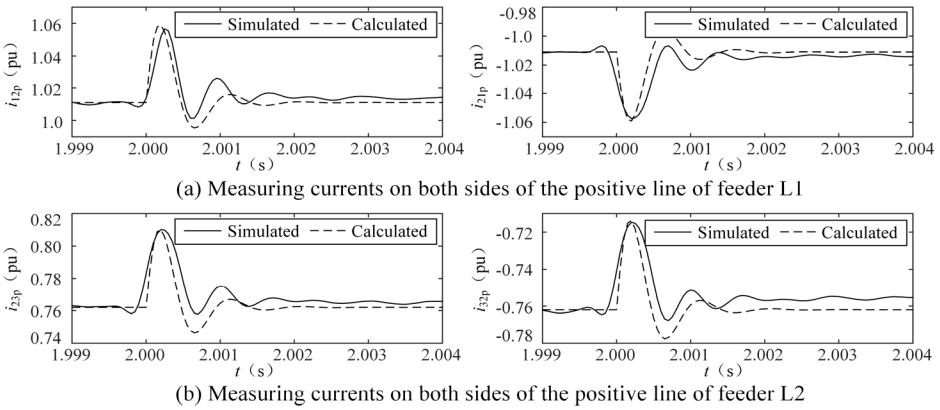

FIGURE 15. Simulation waveforms and calculation results of the positive pole-to-ground fault with 50-ohm transition resistance.

after filtering. For feeder L3, the measuring current near the fault point (i_{34p}) has a negative initial half-wave (so f0 is a reverse fault), while the current near the MMC2 (i_{43p}) has a positive initial half-wave (so f0 is a forward

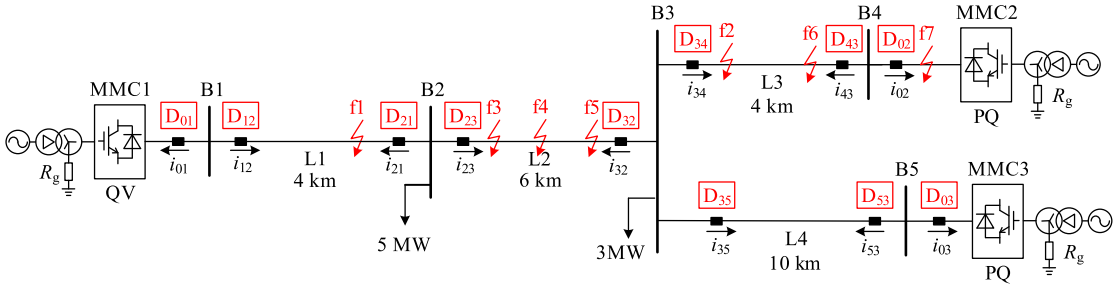

FIGURE 16. Structure of three-terminal simulation system.

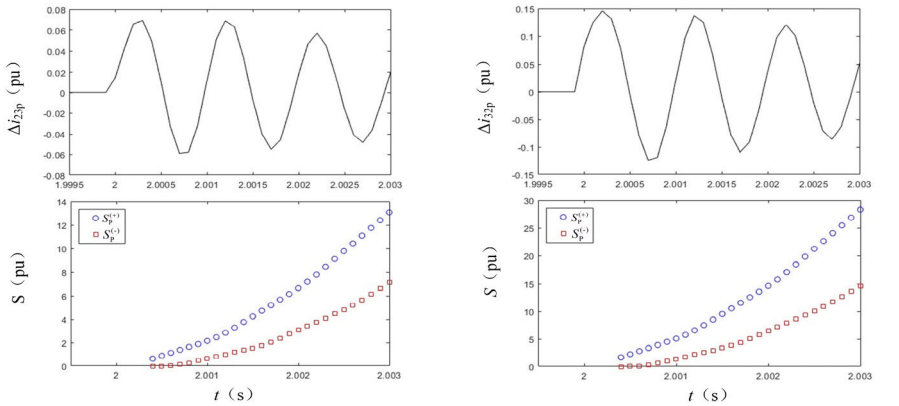

(a) Current fault component and the double integral value at B2 side

(b) Current fault component and the double integral value at B3 side

FIGURE 17. Current fault components and the double integral values on both sides of L2 with a positive metallic ground fault f4.

fault). In summary, the PTG fault current has clear directional characteristics.

Fig. 14 and Fig. 15 show the simulation waveforms and calculation results of the positive PTG fault currents with 10 Ω and 50 Ω transition resistance, respectively. The current waveforms in the figures are filtered to eliminate the effect of high-frequency currents generated by the distributed capacitance of the fault pole. As seen from the figures, the theoretical calculation results agree well with the simulation results for the case with transition resistance. In the case of the PTG fault with transition resistance, the fault current still has evident directional characteristics.

B. SIMULATION OF DIRECTIONAL PILOT PROTECTION SCHEME

In order to better verify the applicability of the proposed directional pilot protection scheme in the multi-terminal FDCDN, the three-terminal simulation model shown in Fig. 16 is constructed based on the double-terminal network shown in Fig. 12. Here, MMC1 adopts the constant DC voltage control method, and the remaining MMCs adopt constant the power control method. Active commands for MMC2 and MMC3 are 15 MW and −5 MW, respectively. The parameters of the MMCs, converters, and feeders have been given in Table 1, and the length of the new feeder L4 is 10km.

Taking the pilot protection of feeder L2 as an example, we can test the performance of the pilot protection by simulating positive or negative PTG faults at different network positions. The sampling frequency is 10 kHz. In the tests, the external fault points are set at L1's end (f1) and L3's head (f2), respectively; the internal fault points are set at L2's head (f3), midpoint (f4), and end (f5), respectively. For MMC lead wire protection, taking the MMC2 lead wire as an example, we set an external fault point (f6) and an internal fault point (f7) near MMC2. In addition to metallic faults, the PTG fault with transition resistance is also considered for testing the protection.

In the case of the metallic ground fault f4 occurring on the positive pole, Fig. 17 shows the positive current fault components (filtered) and their double integral values on both sides. As seen in Fig. 17, both sides of the current fault components have positive initial half-waves. The double integral value of the positive half-wave is higher than that of the negative half-wave. Hence, both sides of the directional elements could judge that a forward fault has occurred. The pilot protection will operate to trip and remove the faulty feeder L2.

When a metallic PTG fault f4 occurs on the negative pole, the negative current fault components and the double integral values on both sides are shown in Fig. 18. The

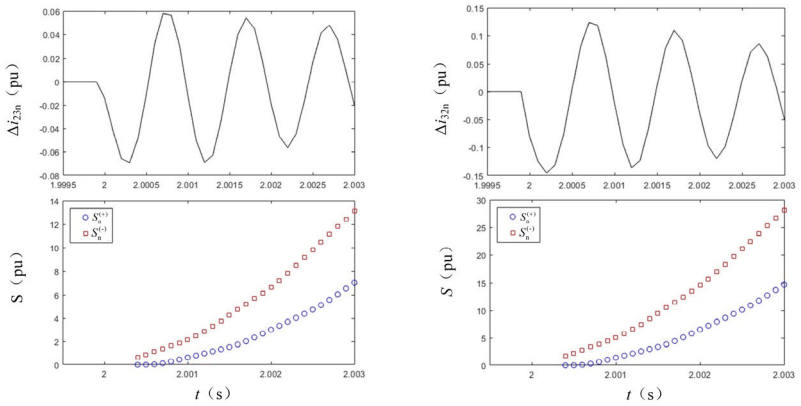

(a) Current fault component and the double integral value at B2 side

(b) Current fault component and the double integral value at B3 side

FIGURE 18. Current fault components and the double integral values on both sides of L2 with a negative metallic ground fault f4.

TABLE 2. Judgment results of the protection with positive metallic ground faults.

Fault location		Directional element D23		Directional element D32		Judgment results of directional pilot protection
		$S_p^{(+)}$ / $S_p^{(-)}$	Judgment results of directional element	$S_p^{(+)}$ / $S_p^{(-)}$	Judgment results of directional element	
Feeder L1	f1	0.420	Reverse	2.084	Forward	External
Feeder L3	f2	1.654	Forward	0.410	Reverse	External
Feeder L2	f3	2.904	Forward	2.132	Forward	Internal
	f4	1.770	Forward	1.903	Forward	Internal
	f5	1.585	Forward	3.155	Forward	Internal

TABLE 3. Judgment results of the protection with negative metallic ground faults.

Fault location		Directional element D23		Directional element D32		Judgment results of directional pilot protection
		$S_n^{(-)}$ / $S_n^{(+)}$	Judgment results of directional element	$S_n^{(-)}$ / $S_n^{(+)}$	Judgment results of directional element	
Feeder L1	f1	0.421	Reverse	2.072	Forward	External
Feeder L3	f2	1.566	Forward	0.423	Reverse	External
Feeder L2	f3	3.032	Forward	2.072	Forward	Internal
	f4	1.805	Forward	1.880	Forward	Internal
	f5	1.566	Forward	3.164	Forward	Internal

fault components on both sides have negative initial half-waves. The double integral value of the negative half-wave is higher than that of the positive half-wave. Both sides of the directional elements could also judge that a forward fault has occurred, and the pilot protection will operate to trip correctly.

When the metallic PTG fault occurs at different positions, the judgment results of the protection are shown in Table 2 and Table 3. The judgment results of the MMC2 lead wire protection are shown in Table 4. As seen from the tables, the directional elements constructed in this paper can correctly

TABLE 4. Judgment results of the mmc lead wire protection.

Fault location (positive pole)		Directional element D34		Directional element D43		Directional element D02		Judgment results of directional pilot protection
		$S_p^{(+)}$ / $S_p^{(-)}$	Judgment results of directional element	$S_p^{(+)}$ / $S_p^{(-)}$	Judgment results of directional element	$S_p^{(+)}$ / $S_p^{(-)}$	Judgment results of directional element	
Feeder L3	f6	1.740	Forward	2.487	Forward	0.402	Reverse	Feeder L3 fault
MMC2 lead wire	f2	1.723	Forward	0.543	Reverse	1.841	Forward	MMC2 lead wire fault
Fault location (negative pole)		Directional element D34		Directional element D43		Directional element D02		Judgment results of directional pilot protection
		$S_n^{(-)}$ / $S_n^{(+)}$	Judgment results of directional element	$S_n^{(-)}$ / $S_n^{(+)}$	Judgment results of directional element	$S_n^{(-)}$ / $S_n^{(+)}$	Judgment results of directional element	
Feeder L3	f6	1.737	Forward	2.555	Forward	0.391	Reverse	Feeder L3 fault
MMC2 lead wire	f2	1.753	Forward	0.537	Reverse	1.862	Forward	MMC2 lead wire fault

TABLE 5. Protection for a positive PTG fault with transition resistance.

Fault location	Transition resistance	D23		D32		Judgment results of directional pilot protection
		$S_p^{(+)}$ / $S_p^{(-)}$	Judgment results of directional element	$S_p^{(+)}$ / $S_p^{(-)}$	Judgment results of directional element	
f1	0Ω	0.420	Reverse	2.084	Forward	External
	10Ω	0.170	Reverse	5.206	Forward	External
	25Ω	0.029	Reverse	30.479	Forward	External
	50Ω	0	Reverse	Inf	Forward	External
	75Ω	0	Reverse	Inf	Forward	External
f2	0Ω	1.654	Forward	0.410	Reverse	External
	10Ω	4.293	Forward	0.171	Reverse	External
	25Ω	42.164	Forward	0.014	Reverse	External
	50Ω	Inf	Forward	0	Reverse	External
	75Ω	Inf	Forward	0	Reverse	External
f4	0Ω	1.770	Forward	1.903	Forward	Internal
	10Ω	4.456	Forward	4.946	Forward	Internal
	25Ω	77.832	Forward	38.346	Forward	Internal
	50Ω	Inf	Forward	Inf	Forward	Internal
	75Ω	Inf	Forward	Inf	Forward	Internal

judge the direction of the fault in 3 ms and have a large margin. The directional pilot protection can distinguish between internal and external faults and reliably remove the faulty feeder.

Tables 5 and 6 give the judgment results of the directional elements and the protection for faults with transition resistance. As seen from the tables, with the increase in transition resistance, the decay of the current fault component accelerates, and the difference between the positive and negative half-waves becomes more apparent ($S_p^{(+)}/S_p^{(-)}$ and $S_n^{(-)}/S_n^{(+)}$ increase). The reliability of the directional criterion and performance of the protection has been further improved. When the transition resistance reaches a considerable value, the short-circuit current will enter the

TABLE 6. Protection for a negative PTG fault with transition resistance.

Fault location	Transition resistance	D23		D32		Judgment results of directional pilot protection
		$S_n^{(-)}/S_n^{(+)}$	Judgment results of directional element	$S_n^{(-)}/S_n^{(+)}$	Judgment results of directional element	
f1	0Ω	0.421	Reverse	2.072	Forward	External
	10Ω	0.169	Reverse	5.167	Forward	External
	25Ω	0.026	Reverse	32.619	Forward	External
	50Ω	0	Reverse	Inf	Forward	External
	75Ω	0	Reverse	Inf	Forward	External
f2	0Ω	1.566	Forward	0.423	Reverse	External
	10Ω	3.857	Forward	0.182	Reverse	External
	25Ω	31.898	Forward	0.015	Reverse	External
	50Ω	Inf	Forward	0	Reverse	External
	75Ω	Inf	Forward	0	Reverse	External
f4	0Ω	1.805	Forward	1.880	Forward	Internal
	10Ω	4.166	Forward	5.030	Forward	Internal
	25Ω	74.775	Forward	37.227	Forward	Internal
	50Ω	Inf	Forward	Inf	Forward	Internal
	75Ω	Inf	Forward	Inf	Forward	Internal

TABLE 7. Judgment results of the protection with positive arc faults.

Fault location		Directional element D23		Directional element D32		Judgment results of directional pilot protection
		$S_p^{(+)}/S_p^{(-)}$	Judgment results of directional element	$S_p^{(+)}/S_p^{(-)}$	Judgment results of directional element	
Feeder L1	f1	0.384	Reverse	2.209	Forward	External
Feeder L3	f2	1.760	Forward	0.376	Reverse	External
Feeder L2	f4	1.830	Forward	1.956	Forward	Internal

over-damped state, and the fault component will be biased to one side of the time axis (as shown in Fig. 6). The difference between the positive and negative half-waves becomes more prominent ($S_p^{(+)}/S_p^{(-)}$ and $S_n^{(-)}/S_n^{(+)}$ tend to infinity), and the protection can correctly distinguish between internal and external faults. In summary, the pilot protection scheme based on comparing positive and negative half-wave integral values of short-circuit current fault components could perform well with high transition resistance.

Arc faults sometimes occur in the network. Due to the susceptibility of arc resistance to various factors such as arc voltage, fault current, and arc length, it is nonlinear and time-varying. However, the change in arc resistance mainly affects the decay rate of the capacitance current. It does not change the current polarity and directional characteristics. At the same time, the arc resistance is small in the initial stage of the fault, while the action time of the protection is short. Therefore, the impact of the time-varying arc resistance on the protection is relatively small. In order to further assess the impact of arc faults on the protection scheme, we conduct simulation tests using an arc model [25]. Table 7 shows the judgment results of the protection scheme with positive arc faults. From Table 7, it can be seen that when an arc fault occurs, the directional characteristics of the fault current will not change, and the protection scheme can still operate correctly.

C. COMPARATIVE ANALYSIS WITH EXISTING PROTECTION SCHEMES

In order to further verify the performance of the proposed protection scheme, we make a comparison with existing protection schemes. The protection scheme based on the frequency domain characteristics of transient zero-mode current proposed in [18] has high requirements on the sampling

TABLE 8. Judgment results of the protection scheme in [16] with positive metallic ground faults.

Fault location (for the differential protection of feeder L2)		the amount of transferred capacitance charges	Judgment results
Feeder L1	f1	-0.323	External fault
Feeder L3	f2	-0.401	External fault
Feeder L2	f4	1.851	Internal fault
Fault location (for MMC2 lead wire)		the amount of transferred capacitance charges	Judgment results
MMC2 lead wire	f7	/	/

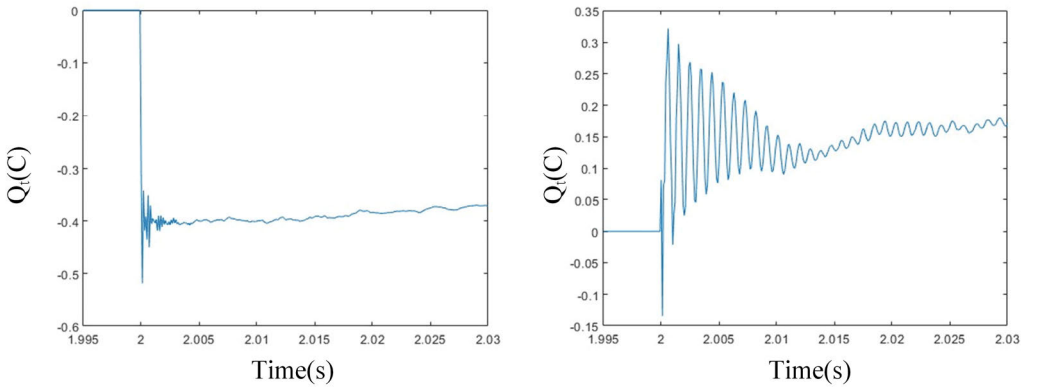

(a)the amount of transferred capacitance charges in strict sampling synchronization

(b)the amount of transferred capacitance charges with 0.2ms sampling synchronization error

FIGURE 19. Simulation results of the feeder L2 differential protection when positive PTG fault occurs at f2.

frequency (not less than 25kHz). It is hard to apply in engineering. He et al. [19] proposes a protection idea based on comparing the initial traveling wave polarity. However, the reference does not give specific protection criteria and implementation methods. At the same time, the valid time of the initial traveling wave is short, so the reliability of the protection needs to be improved. Therefore, we select [16], the differential current protection, and compare it with the directional pilot protection proposed in this paper.

Li et al. [16] uses the transient differential current to calculate the amount of transferred capacitance charges to distinguish between internal and external faults. Suppose the current sampling on both sides of the feeder is strictly synchronized. The simulation results of the protection with positive metallic faults are shown in Table 8. The simulation results show that when a PTG fault occurs, the protection could operate correctly in most cases. However, when the fault occurs at the MMC lead wire (f7), the differential protection will fail to remove the fault since only one side current can be obtained. In contrast, the protection scheme proposed in this paper can still operate correctly, as shown in Table 4.

Another major problem in the practical application of the protection scheme is the strict requirement for sampling synchronization on both sides of the feeder. If there is an error in sampling synchronization, it may lead to protection rejection or misoperation. Taking the occurrence of positive PTG fault at point f2 in Fig. 16 as an example, the simulation results of the feeder L2 differential protection are shown in Fig. 19. From the figure, the amount of transferred capacitance charges is negative in the case of strict sampling synchronization. The fault can be correctly judged as external, and the protection does not operate. When the sampling synchronization error is 0.2ms, the calculated amount of transferred charges is positive. The fault will be misclassified as internal, causing the protection misoperation. In contrast, the direction element proposed in this paper only needs the local information to judge the fault direction without sampling synchronization. It is convenient for engineering.

In summary, compared with the transient current differential protection scheme, the directional pilot protection scheme proposed in this paper has superiority regarding grid line applicability and sampling synchronization requirements.

V. CONCLUSION

According to the characteristics of FDCDN, this paper studies the PTG fault characteristics and the novel protection scheme. The main contributions and conclusions are as follows:

(1) According to the structure and characteristics of FDCDN, an equivalent PTG fault model is established, and the analytical expression of short-circuit current is derived. The simulation results of the fault current verify the correctness of the theoretical analysis method, which lays the foundation for PTG fault characteristic analysis and protection scheme research.

(2) The fault analysis results show that the steady-state short-circuit current is very small and hard to detect due to the pseudo-bipolar structure. Therefore, for the PTG fault, it is appropriate to use the transient fault component of the short-circuit current for fault detection. The transient fault component is mainly the distributed capacitance current, of which the non-fault pole capacitance current has a low frequency and a long duration. At the same time, the difference between its positive and negative half-waves is prominent in the case of forward or reverse faults. Therefore, the non-fault pole capacitance current has prominent directional characteristics and can be used to determine the fault direction.

(3) This paper proposes a novel directional pilot protection scheme based on the double integration of short-circuit current fault components. The scheme determines the fault direction by comparing the double integral values of positive and negative half-waves. The simulation results show that the scheme can reliably identify faulty lines and perform well with high transition resistance. Also, the directional elements on both sides of the feeder only use local information to determine the direction of the fault without sampling synchronization. They do not need the current information from the opposite side. The protections on both sides of the feeders only need to exchange logical information about the fault direction judgment results. The communication volume is low, and the influence of communication time delay and jitter is small. There is no requirement for special compensation, and wireless communication can be used at a low cost. Therefore, the scheme is easy to be applied in engineering.

For PTG fault protection in FDCDN, this paper proposes a novel directional pilot protection scheme and verifies its feasibility by simulation. Next, we will carry out further research in the following aspects:

(1) An outstanding advantage of the protection scheme is the low requirement for the communication system so that wireless communication technology can be used. In the next step, we will combine wireless communication technology to research relevant communication interfaces, protocols, etc. For possible problems like incorrect and lost codes, we will propose relevant solutions to meet the application requirements of the protection.

(2) We will research the corresponding relay protection devices based on the proposed protection scheme. To realize their engineering application, we will conduct comprehensive experimental tests on the devices in terms of protection performance and device reliability.

TABLE 9. Definitions.

FDCDN	Flexible DC distribution network
PTG	Pole-to-ground
PTP	Pole-to-pole
MMC	Modular multilevel converter

APPENDIX

The definitions used in this paper are shown in Table 9.

REFERENCES

[1] J. Daozhuo and Z. Huan, "Research status and developing prospect of DC distribution network," *Automat Electr Power Syst.*, vol. 36, no. 8, pp. 98–104, Apr. 2012.
[2] M. Starke, F. Li, L. M. Tolbert, and B. Ozpineci, "AC vs. DC distribution: Maximum transfer capability," in *Proc. IEEE Power Energy Soc. Gen. Meeting Convers. Del. Electr. Energy 21st Century*, Jul. 2008, pp. 1–6.
[3] M. Starke, L. M. Tolbert, and B. Ozpineci, "AC vs. DC distribution: A loss comparison," in *Proc. IEEE/PES Transmiss. Distrib. Conf. Expo.*, Apr. 2008, pp. 1–7.
[4] F. Dastgeer and A. Kalam, "Efficiency comparison of DC and AC distribution systems for distributed generation," in *Proc. AUPEC*, 2009, pp. 1–5.
[5] S. H. Lee, Y. C. Kang, and J.-W. Park, "Optimal operation of multiple DGs in DC distribution system to improve system efficiency," *IEEE Trans. Ind. Appl.*, vol. 52, no. 5, pp. 3673–3681, Sep. 2016.
[6] G. Liu, Y. Zhao, Z. Yuan, B. Zhao, Z. Yu, Z. Si, G. Sun, X. Xu, Y. Han, Q. He, and M. Chen, "Study on demonstration project technical scheme of VSC-DC distribution system in Shenzhen," *Southern Power Syst. Technol.*, vol. 10, no. 4, pp. 1–7, Apr. 2016.
[7] M. Stieneker, J. Butz, S. Rabiee, H. Stagge, and R. W. D. Doncker, "Medium-voltage DC research grid Aachen," in *Proc. Int. ETG Congr., Die Energiewende, Blueprints New Energy Age*, Bonn, Germany, Nov. 2015, pp. 1–7.
[8] J. C. Das and R. H. Osman, "Grounding of AC and DC low-voltage and medium-voltage drive systems," *IEEE Trans. Ind. Appl.*, vol. 34, no. 1, pp. 205–216, Jan./Feb. 1998.
[9] J. Zhang, C. Zhao, X. Huang, Y. Lu, and P. Qiu, "Simulation research on earth fault characteristics of modular multilevel converter based high voltage direct current transmission system," *Power Syst. Technol.*, vol. 38, no. 10, pp. 2658–2664, Oct. 2014.
[10] C. Zhao, T. Li, L. Yu, Y. Huang, L. Li, and X. Li, "DC pole-to-ground fault characteristic analysis and converter fault recovery strategy of MMC-HVDC," *Proc. CSEE*, vol. 34, no. 21, pp. 3518–3526, Jul. 2014.
[11] Z. Dai, C. Zhang, X. Chen, and Y. Li, "Fault analysis of multi-terminal flexible DC distribution system with RES," in *Proc. IEEE PES Asia–Pacific Power Energy Eng. Conf. (APPEEC)*, Oct. 2018, pp. 589–594.
[12] J. Li, Y. Zhang, Q. Zeng, K. Chen, and H. Tian, "Pole-to-ground fault current calculation method for MMC-MTDC systems," *Power Syst. Technol.*, vol. 43, no. 2, pp. 546–553, Feb. 2019.
[13] N. Chen, L. Qi, X. Cui, and J. Ma, "Calculation method for line-to-ground short-circuit currents of VSC-HVDC grid," *Electr. Power Construct.*, vol. 40, no. 4, pp. 119–127, Apr. 2019.
[14] L. Liu, X. Kang, M. Zheng, and K. Li, "A fast protection scheme using fault current characteristics in multi-terminal flexible DC distribution network," in *Proc. IEEE 8th Int. Conf. Adv. Power Syst. Autom. Protection (APAP)*, Oct. 2019, pp. 317–321.
[15] G. Song, Z. Chang, C. Zhang, S. T. H. Kazmi, and W. Zhang, "A high speed single-ended fault-detection method for DC distribution line—Part II: Protection scheme," *IEEE Trans. Power Del.*, vol. 35, no. 3, pp. 1257–1266, Jun. 2020.

[16] B. Li, X. Ren, and B. Li, "Study on the charge transfer criterion for the pole-to-ground fault in DC distribution networks," *IEEE Access*, vol. 7, pp. 102386–102396, 2019.
[17] T. Bi, S. Wang, K. Jia, Z. Zhou, and W. Li, "Short-term energy based approach for monopolar grounding line identification in MMC-MTDC system," *Power Syst. Technol.*, vol. 40, no. 3, pp. 689–695, Mar. 2016.
[18] C. Yang, S. Lin, and M. Guo, "Multi-frequency bands based pole-to-ground fault detection method for MMC-based radial DC distribution systems," *Int. J. Electr. Power Energy Syst.*, vol. 141, Oct. 2022, Art. no. 108250.
[19] S. He, G. Zou, C. Sun, and S. Liu, "Fault section locating method and recovery strategy of pole-to-ground fault for medium voltage direct current (MVDC) distribution network," *J. Eng.*, vol. 2019, no. 16, pp. 668–673, Mar. 2019.
[20] G. Sun, B. Shi, and Y. Zhao, "Research on the fault location method and protection configuration strategy of MMC based DC distribution grid," *Power Syst. Protection Control*, vol. 43, no. 22, pp. 127–133, Nov. 2015.
[21] R. Xu, Z. Chang, G. Song, J. Hou, N. Chang, and P. Chang, "Grounding fault identification method for DC distribution network based on detection signal injection," *Power Syst. Technol.*, vol. 45, no. 11, pp. 4269–4276, Nov. 2021.
[22] X. Feng, L. Qi, and J. Pan, "A novel fault location method and algorithm for DC distribution protection," *IEEE Trans. Ind. Appl.*, vol. 53, no. 3, pp. 1834–1840, May 2017.
[23] S. D. A. Fletcher, P. J. Norman, K. Fong, S. J. Galloway, and G. M. Burt, "High-speed differential protection for smart DC distribution systems," *IEEE Trans. Smart Grid*, vol. 5, no. 5, pp. 2610–2617, Sep. 2014.
[24] K. Jia, C. Wang, T. Bi, R. Zhu, and Z. Xuan, "Transient current waveform similarity based protection for flexible DC distribution system," *IEEE Trans. Ind. Electron.*, vol. 66, no. 12, pp. 9301–9311, Dec. 2019.
[25] J. L. Guardado, S. G. Maximov, E. Melgoza, J. L. Naredo, and P. Moreno, "An improved arc model before current zero based on the combined Mayr and Cassie arc models," *IEEE Trans. Power Del.*, vol. 20, no. 1, pp. 138–142, Jan. 2005.

HAO QI received the B.S. degree from Shandong University, Jinan, China, in 2021. She is currently pursuing the M.S. degree in electrical engineering with the Huazhong University of Science and Technology. Her research interests include operation control and protection technology of DC distribution networks.

WEI CHEN (Member, IEEE) received the Ph.D. degree in electrical engineering from the Huazhong University of Science and Technology, Wuhan, China, in 2004. He is currently an Associate Professor at the Huazhong University of Science and Technology. His research interests include control and protection for AC/DC transmission and distributed/renewable energy generation.

ZHENLAN DOU (Member, IEEE) received the Ph.D. degree in electrical engineering from Shanghai Jiao Tong University, in 2013. She is currently a Senior Engineer, the Technical Director, and the Director Assistant of State Grid Shanghai Municipal Electric Power Company. Her research interests include integrated energy systems and its control technology research, distributed energy systems, urban energy internet, hydrogen energy, energy storage, wind, and other new energy power generation systems and their control.

JIEXIANG HAN received the Ph.D. degree in electronic engineering from the Huazhong University of Science and Technology, Wuhan, China, in 2022. He is currently an Engineer with State Grid Gansu Electric Power Company. His research interests include operation control and protection technology of AC–DC hybrid networks.

PEI SUN received the M.S. degree from Jilin University, China. She is currently with the State Grid Shanghai Electric Power Research Institute. Her research interests include protective relaying and coordination between the power grid and source.

ZHE ZHANG received the Ph.D. degree in electrical engineering from the Huazhong University of Science and Technology (HUST), Wuhan, China, in 1991. He is currently a Professor with the College of Electrical and Electronic Engineering, HUST. His research interests include power system analysis and protective relaying.

XIANGGEN YIN (Senior Member, IEEE) received the B.S., M.S., and Ph.D. degrees in electrical engineering from the Huazhong University of Science and Technology (HUST), Wuhan, China, in 1982, 1985, and 1989, respectively. He is currently a Professor with the School of Electrical and Electronic Engineering, HUST. His research interests include power system analysis, fault location, protective relaying, and power system stability control.